Materials Chemistry and Physics 162 (2015) 548–554

Contents lists available at ScienceDirect

Materials Chemistry and Physics

journal homepage: www.elsevier.com/locate/matchemphys

A one-step method to coat polystyrene particles with an organo-silica shell and their functionalization

Tian-Song Deng [a], [*], Hans-Josef Bongard [a], Frank Marlow [a], [b], [**]

[a] Max-Planck-Institut für Kohlenforschung, Kaiser-Wilhelm-Platz 1, 45470 Mülheim an der Ruhr, Germany
[b] Center for Nanointegration Duisburg-Essen (CENIDE), University of Duisburg-Essen, 47057 Duisburg, Germany

HIGHLIGHTS

- Demonstrated a one-step controllable coating method of organo-SiO_2 on polystyrene.
- The Br-modified PS@vinyl-SiO_2 colloidal crystal has tunable photonic band gaps.
- PS@mercaptopropyl-SiO_2 particles allow the encapsulation of small Au nanoparticles.

ARTICLE INFO

Article history:
Received 13 February 2015
Received in revised form
10 June 2015
Accepted 14 June 2015
Available online 21 June 2015

Keywords:
Coatings
Optical materials
Thin films
Sol–gel growth
Surface properties

GRAPHICAL ABSTRACT

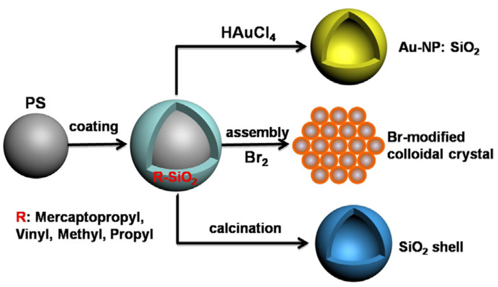

ABSTRACT

A facile method of coating polystyrene (PS) particles with organo-silica and their functionalization was presented. By adding the organo-silane precursor into PS aqueous solution in presence of ammonia, an organo-silica shell could be coated on PS particles directly. This method has several characteristics. First, only one process, one precursor and one solvent were used. Second, the organic groups could be varied from methyl, propyl, vinyl, to mercaptopropyl. The third is the tunable shell thickness with a high monodispersity. The organo-silica shells are further functionalized. The PS@vinyl-SiO_2 particles were used to assemble colloidal crystals, and further modified with bromine, resulting in tunable photonic band gaps. PS@mercaptopropyl-SiO_2 particles allow the encapsulation of Au nanoparticles. The resulting 2.2 nm Au particles were stable at 550 °C and well-distributed in the whole SiO_2 shell with a loading up to 20 wt%.

1. Introduction

Core-shell particles have attracted considerable attention in physics, chemistry, and medicine, due to their application potential in photonic crystals, catalysis, and drug delivery [1–6]. Extrapolating these interesting works, one may envisage tunable optical systems usable as breadboards of photonic integrated circuits or geometrically designed catalysts for consecutive chemical reactions. In the developments, PS@SiO_2 is a popular basic core—shell system [7–11]. The PS core can have a highly uniform spherical shape, a high monodispersity, and a possible inner core—shell structure as well. Also the PS can easily be removed via chemical leaching or calcination, and then hollow particles [10,11] or yolk-shell systems can be obtained. The SiO_2 shell is usually fabricated by a Stöber-like method [12] delivering a controllable homogeneous thickness and a tunable porosity [1–3]. In addition,

---

[*] Corresponding author.
[**] Corresponding author. Max-Planck-Institut für Kohlenforschung, Kaiser-Wilhelm-Platz 1, 45470 Mülheim an der Ruhr, Germany.
E-mail addresses: dengts@pku.edu.cn (T.-S. Deng), marlow@mpi-muelheim.mpg.de (F. Marlow).

http://dx.doi.org/10.1016/j.matchemphys.2015.06.027

owning to the negative charge, SiO_2 can prevent the aggregation of the colloidal particles. However, commonly used PS particles are also negatively charged [13]. Therefore, it's hard to get smooth and homogeneous coating of SiO_2 directly on the negatively charged PS particles. Many groups have developed different ways to modify the surface of PS particles, e.g. SiOH-functionalized surfaces [8], PVP-stabilized surfaces [9], and polyelectrolyte deposited (positively charged) surfaces [13]. It takes two or even more steps, which are very time-consuming in reaction and cleaning process.

One application of core–shell systems is photonic band gap materials. Such materials require a high monodispersity of the building blocks and a usable chemical flexibility to tune the system towards applications such as photonic waveguides or resonators. Monodispersity and tuning abilities were achieved in several works, e.g. PNIPAM-based thermo-responsive colloidal crystals [14,15]. However, temperature and most chemical tunings lead to lattice constant changes, which can be acceptable for sensor applications but not for application in many other photonic devices. They destroy the device or induce defects. Therefore, constant-lattice tuning possibilities are required. The refractive index of the building blocks has to be changed, but the geometry should stay constant. The functionalization of core–shell systems is now an important way to connect them with optically active ligands in a flexible manner.

Another interesting application could be catalysis. Noble metals grafted on inorganic matrices are widely investigated. Especially gold nanoparticles (Au-NPs) are often used for the catalytic applications [16–24]. Different ways have been applied to graft Au-NPs on or in SiO_2 matrix particles. One way is to infiltrate Au ions into mesoporous SiO_2 spheres being the host for the formation of Au-NPs inside the pores [16–18]. Another way is the use thiol groups [20,22,24]. For example, a series of organically functionalized core–shell spheres was synthesized [22] which fixed the Au-NPs on the core surface by the binding between thiol and Au. However, two problems have been recognized for such systems. First, the migration of Au-NPs leads to aggregation and to a loss of catalytic activity at elevated temperatures (about 200 °C) [16–18]. Also Au-NPs protected by a shell of SiO_2 cannot endure much higher temperatures [22]. The second problem is the low loading with Au-NPs especially for low-surface area materials [24]. High and temperature-stable loading is therefore a challenge for many Au-NP containing catalysts.

Recently, we reported a method to synthesize monodisperse PS@v-SiO_2 core–shell particles, by using PS particles as template and vinlytrimethoxysilane (VTMS) as the precursor [25]. The procedure involved the pre-hydrolysis of VTMS precursor in water and then directly coating vinyl-SiO_2 on the PS surface at room temperature. In this paper, we develop a one-step method to coat PS particles with organo-SiO_2 (Scheme 1). By elevating the reaction temperature, pre-hydrolysis of the precursor is not necessary. The reduction of this two-step procedure to one-step makes it easier to generalize this approach to flexible organic ligands. In addition, the enhanced temperature enables the use for several organo-silanes, which are strongly hydrophobic and hard to be dispersed in cold water. Subsequent modifications demonstrate the accessibility of the functional groups and the efficient tunability of these building blocks. For example, PS@v-SiO_2 core–shell systems were modified with bromine leading to efficiently tunable colloidal crystals with stable lattices. Furthermore, Mercaptopropyl-SiO_2 shells were impregnated with $HAuCl_4$ forming a high loading of well-distributed Au-NPs inside the SiO_2 shell.

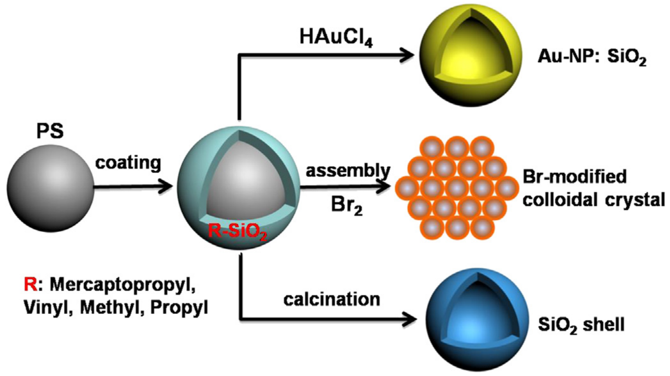

Scheme 1. One-step R–SiO_2 coating on PS and their functionalization to form Au-NP: SiO_2, Br-modified colloidal crystal, and hollow SiO_2 shell.

2. Experimental section

2.1. Materials

Methyltrimethoxysilane (MTES, 99%), n-Propyltriethoxysilane (n-PrTES, 97%), vinyltrimethoxysilane (VTMS, 98%), 3-Mercaptopropyl trimethoxysilane (MPTMS, 95%), and bromine (≥99.5%) were purchased from Sigma–Aldrich. Ammonia solution ($NH_3 \cdot H_2O$, 28–30%) and Ethanol (99.9%) were purchased from Merck. PS particles (284 nm in diameter, terminated with sulfate groups, negatively charged) were purchased from Microparticles GmbH (Berlin). All chemicals were used as received. Ultrapure water was used directly from a Milli-Q water system.

2.2. PS@Organo-SiO_2 core–shell particles

Core-shell particles were prepared by coating an organo-SiO_2 shell on the surface of PS core via a modified Stöber process that involved hydrolysis and condensation of the organo-silane in aqueous solution. For the PS@methyl-SiO_2 particles, 15 mL 0.5 wt% of PS aqueous suspension was heated to 60 °C under stirring, and then 10 mL ammonia solution was added. After 5 min, 0.5 mL MTES was dropped into the PS/NH_3/H_2O system. The reaction was allowed to proceed for 5 h at 60 °C. The resulting particles were washed three times with ethanol. For the n-PrTES/MPTMS precursor, 30 mL 0.25 wt% PS was used. The processes were the same as the MTES synthesis. The details are listed in Table 1.

2.3. Hollow SiO_2 shells

The hollow SiO_2 shells were obtained after removing the PS core. The core–shell particles were heated to 550 °C with a rate of 2 °C/min in air, kept for 6 h, and then cooled to room temperature. The obtained hollow SiO_2 shells were dispersed in ethanol for further use.

2.4. Br-modified colloidal crystals

The colloidal crystals were fabricated by using the capillary deposition method [6]. A suspension of 0.5 wt% PS@v-SiO_2 particles (sample DNT-DA-071-01, shell thickness 104 nm) in ethanol was used. The planar capillary cell was consisted of two glass slides separated by two polymer spacers (15 μm). A capillary tube was connected the colloidal suspension and the lower glass plate. The suspension was dragged up into the cell due to the capillary force. The colloidal crystal film was formed after evaporation of the solvent at the open edges of the capillary cell. For the bromine modification, a 2% (v/v) bromine solution in ethanol was infiltrated into the crystal via the capillary tube instead of the suspension. The infiltration was allowed to process 24 h. After infiltration, the cell

Table 1
Core-shell spheres obtained from different organo-silanes.

No.	Organic group	Precursor	C_{o-Si} (mL)	$D_{o\text{-}Si}$ (nm)	P_{o-Si} (%)	$t_{o\text{-}Si}$ (nm)
1	Methyl	MTES	0.5	343	2.6	34.1 ± 4.1
2	Propyl	PrTES	0.6	418	2.9	74.3 ± 6.1
3	Vinyl	VTMS	0.4	343	2.4	40.1 ± 4.2
4	Mercaptopropyl	MPTMS	0.5	483	2.4	104.1 ± 6.5

$D_{o\text{-}Si}$, P_{o-Si}, and $t_{o\text{-}Si}$: mean diameter, polydispersity and shell thickness of PS@organo-SiO_2 core–shell particles. The polydisperity P_{o-Si} is defined by the relative standard deviation of the diameter.

was dried in air for several days. *Note: Bromine is highly toxic and very volatile and needs to be handled with caution.*

2.5. 0@Au-NP:SiO_2 shell particles

The PS@mp-SiO_2 dispersion was dried at 50 °C overnight. Then 5 mg of the PS@mp-SiO_2 powder was added to 30 mL 0.05 wt% of $HAuCl_4$ aqueous solution. The contents were briefly sonicated for 2 min and then stirred at 80 °C for 24 h. A part of the particles formed a sediment layer at the bottom. All particles were separated by centrifugation, washed 3 times with H_2O. A part of these particles were analyzed, the others were calcined at 550 °C for 6 h. The resulting powder (named 0@Au-NP:SiO_2 shells) was used for analysis without further purification.

2.6. Characterization

The morphology of particles was observed by a transmission electron microscope (TEM) (Hitachi HF 2000). To prepare the samples, a carbon coated copper grid were dipped in the particle dispersion and drying in air. The geometric parameters of the particles were measured for about 100 particles for each TEM image.

The colloidal crystal films were observed using scanning electron microscopy (SEM) (Hitachi S-3500N). A gold layer (10 nm) was sputtered on the film before observing. A Cary 5G UV–vis–NIR spectrometer (Varian) was used for measuring the transmission spectra of the colloidal crystal films (15 μm thick).

The Au-NPs encapsulated samples were also characterized by a scanning transmission electron microscope (Hitachi S-5500) working in transmission dark field mode (DF), transmission bright field mode (BF), or normal secondary electron (SE) mode. A high acceleration voltage of 30 kV was used for all modes. Color processing of selected pictures was carried out by the Hitachi S-5500 software.

In some cases, sections were cutted with a Reichert Ultracut ultra-microtome. The particles were fixed in a Spurr resin (hard mixture), and a series of thin sections of the particles with the thickness of about 28 nm were prepared and transferred onto a copper grid with a lacey film. EDX of the 0@Au-NP:SiO_2 shell with mapping of the distribution of O, Si, and Au in a 0@Au-NP:SiO_2 through different directions was performed by a Noran System 7 x-ray Microanalysis System (Thermo Scientific) coupled to a Hitachi S-5500.

3. Results and discussion

Fig. 1 shows TEM images of the synthesized PS@organo-SiO_2 core–shell particles with different organo-SiO_2 shells. All 4 kinds of particles have a polydispersity lower than 3% and thickness fluctuations lower than 12%. Particle size, polydispersity, and shell thickness of the core–shell particles are listed in Table 1. We emphasize the different chemical character of the functional groups. The thickness of the organo-SiO_2 shell can easily be controlled by several parameters, such as reaction temperature, reaction time, precursor concentration, pH, and the ratio of the precursor and PS as it was shown for some examples [25,26]. Here, we fixed the other parameters and used the influence of precursor concentration only. TEM images of the PS@v-SiO_2 core–shell particles with different amount of VTMS precursor are given in the supporting information (Fig. S1). By increasing the VTMS amount, the shell thickness could be adjusted in the range of 10 nm–110 nm, without losing the monodispersity and the uniformity of the shells. This confirms the controllability of the coating process. The elevated reaction temperature improves the coating process and makes the coated shells more perfect in comparison to a former work [25]. There, more eccentric shells have occurred.

The core–shell systems can also be used to fabricate hollow shells. For this, core–shell particles were treated at 550 °C for 6 h. The PS templates burned away and well-shaped SiO_2 shells remained (Fig. 2). The hollow shells are still highly monodisperse ($P < 3\%$) despite the large shrinkage of particle size and shell thickness (see Table S2). The calcination experiments show the integrity and the accessibility to chemical reactions for all these organo-SiO_2 shells. Due to the high monodispersity and the redispersibility of the particles, the hollow SiO_2 shells can be used for growing colloidal crystals. The resulting crystals show a reduced number of defects. This interesting point is addressed in another study [27].

Compared to the normal SiO_2, the organo-SiO_2 easily allows further homogeneous modification of the material due to the homogeneous presence of the organic groups [28–30]. Normally, post-synthesis coating with triethoxysilanes (RTES) or trimethoxysilanes (RTMS) has been used for functionalization, where the R represents different organic substitutes [28]. However, this post-synthesis functionalization results in thin active layers on the accessible SiO_2 surface only. Using the whole volume of the synthesized material is very difficult. Thus, the organo-SiO_2 shells represent a convenient starting point for further material design. In the following, we will give an example of shell modifications using the organic groups in the shells.

Due to the PS core and the vinyl groups in the v-SiO_2 shell, colloidal crystals composed of PS@v-SiO_2 particles offer different tuning possibilities for their photonic properties. The vinyl groups can be used for addition reactions, e.g. with bromine or borane hydride [31]. In former reports, temperature-tuning was investigated for colloidal crystals of v-SiO_2 [32] and PS@v-SiO_2 [25]. The stop band showed a large blue-shift, mainly due to the shrinkage of the particles after the temperature treatment. However, this also caused a large number of cracks, leading to a broadening of the Bragg peak and a poor crystalline quality.

The tuning the optical properties via chemical addition reactions can avoid the crack formation during tuning. Therefore, we examined modification of the v-SiO_2 shells with bromine. The colloidal crystals were fabricated from PS@v-SiO_2 particles via the capillary deposition method [6]. As seen in Fig. 3a, well-packed arrays were formed, with regular linear cracks in the sub-micron range. Then, the PS@v-SiO_2 colloidal crystals were treated with

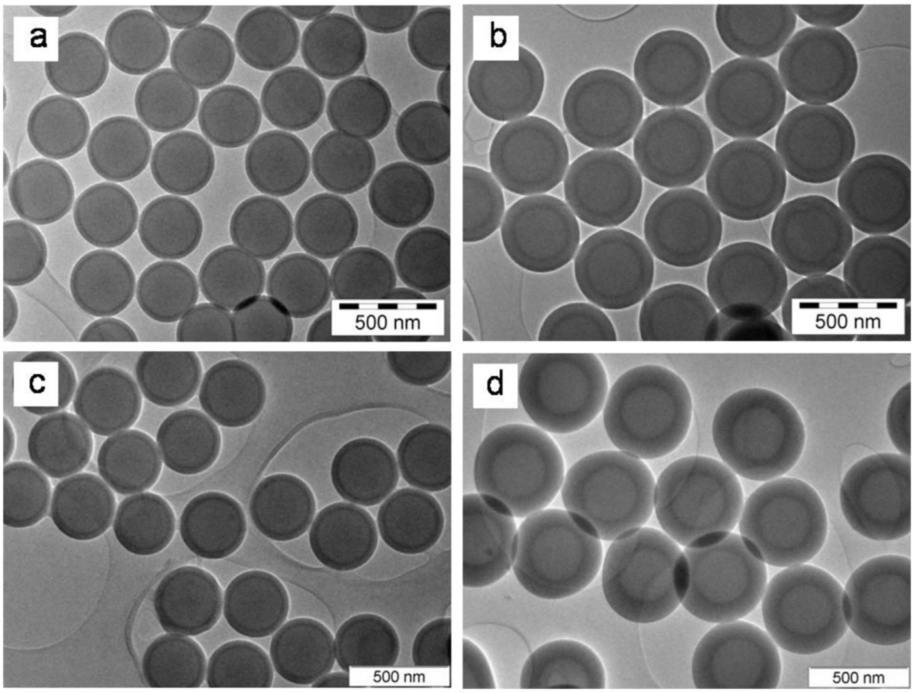

Fig. 1. TEM images of PS@organo-SiO_2 particles with different organic groups: (a) methyl, (b) propyl, (c) vinyl, and (d) mercaptopropyl.

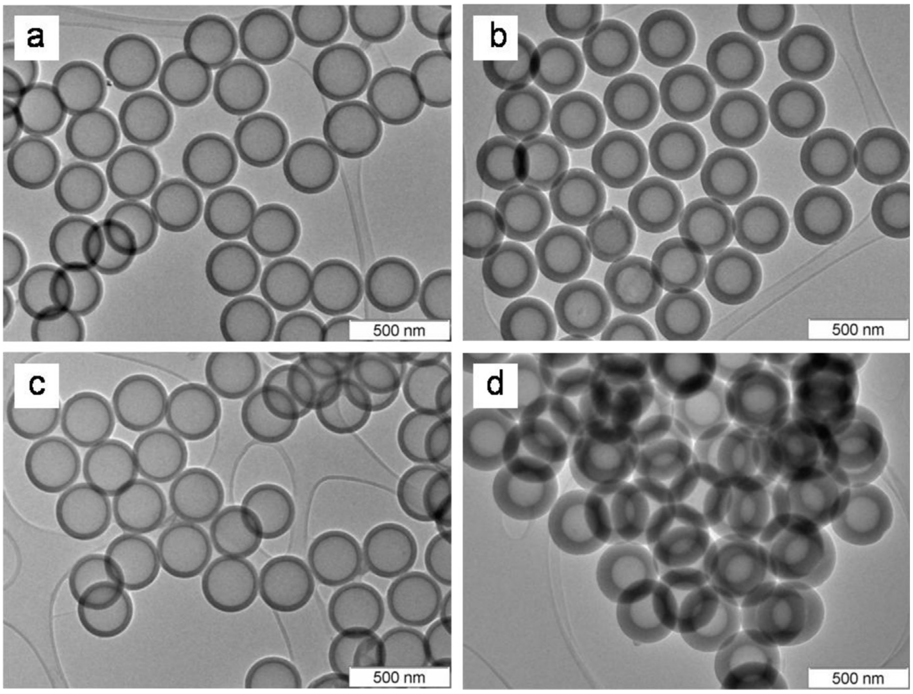

Fig. 2. TEM images of hollow SiO_2 shells obtained by calcination of different PS@R-SiO_2 core–shell particles: R = methyl (a), propyl (b), vinyl (c), and mercaptopropyl (d). These hollow shells were obtained the same core–shell particles as shown in Fig. 1.

bromine in ethanol and dried in air. Fig. 3b shows the arrays of the Br-modified colloidal crystals. The lattice of Br-modified colloidal crystal is seemingly unchanged in all properties, in the structure, in the lattice constant, and in the crystalline quality (see more SEM images in Fig. S2). However, the optical properties show obvious changes as visible in Fig. 4. The stop band (Bragg peak) is red-shifted from 1076 nm to 1163 nm after the Br modification. Due to the unchanged lattice constant, this is connected with the increase of the effective refractive index.

Under normal incidence, the diffracted wavelength is given by the Bragg equation involving an effective refractive index n_{eff} [6].

$$\lambda_B = 2n_{eff}d_{111} \tag{1}$$

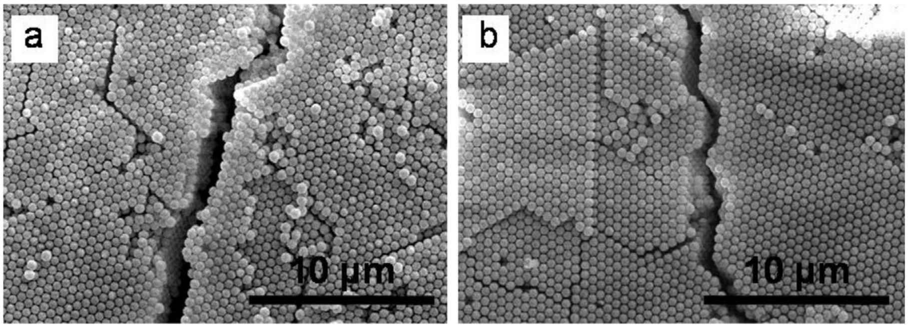

Fig. 3. SEM images of (a) PS@v-SiO_2 colloidal crystals, and (b) Br-modified colloidal crystals. The lattice constant is 695 nm for both.

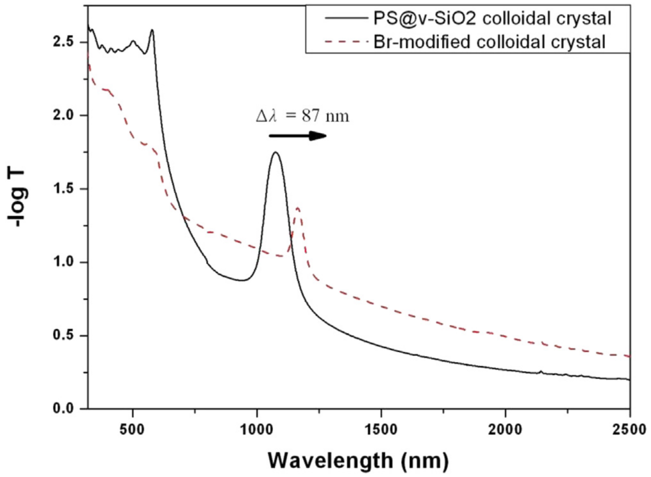

Fig. 4. Transmission spectra of a PS@v-SiO_2 colloidal crystal and a Br-modified colloidal crystal. A red-shift of Bragg peak of $\Delta\lambda = 87$ nm was observed. (For interpretation of the references to color in this figure legend, the reader is referred to the web version of this article.)

$$n_{eff}^2 = n_a^2 f_a + n_c^2 f_c + n_{sh}^2 f_{sh} \tag{2}$$

$$f_a = 0.26,\ \ f_c = 0.74\frac{D_c^3}{D_{sh}^3},\ \ f_{sh} = 0.74\frac{D_{sh}^3 - D_c^3}{D_{sh}^3} \tag{3}$$

where λ_B is the Bragg peak wavelength, d_{111} is the (111) plane distance which depends on the lattice constant. The effective refractive index depends on the refractive indices of the core n_c (=1.59 for PS), of the shell n_{sh}, and of the ambient medium n_a (=1 for air). f_c, f_{sh}, and f_a are the volume fractions of the corresponding parts in the lattice. D_{sh} and D_c are the diameters of the whole core@shell sphere and of the core part, respectively. In Equation (3) the ideal packing of the core@shell spheres was assumed. From (1)–(3), one finds $n_{sh} = 1.415$ for the unmodified v-SiO_2 shells, and $n_{sh} = 1.584$ for the Br-v-SiO_2 shells. The result for v-SiO_2 is a bit lower than for normal SiO_2, which we ascribe to the porosity of the shells. The Br-modification causes an increase of n_{sh} by $\Delta n_{sh} = 0.17$. This is quite a large effect which is able to influence the propagation of light by these nanoparticles efficiently.

The geometrical rigidity of the system used for the above calculation is not only indicated by the SEM observations but also understandable by the construction of the material. The organosilica forms a 3D network interconnected with organic groups. The organic groups are bound to the network only by one bond. Changes in the organic group therefore have a very small influence on the 3D network.

The increase of the refractive index of the shell by bromine is, of cause, an expected effect. It is observed in bromine-containing liquids and polymers [33,34] and it can be ascribed to the higher molar refraction contributions of the two Br atoms replacing one C=C double bond. For instance, Roll et al. [34] calculated a refractive index of 1.7 for $[2,5\text{-}Br_2PhSiO_{1.5}]_8$ crystals. The Clausius–Mossotti equation relates the refractive index n of a substance to its polarizability which can be described by the molar refraction [33].

$$\frac{n^2 - 1}{n^2 + 2} = \frac{R_m}{V_m} \tag{4}$$

Here R_m is the molar refraction and V_m stands for the molar volume. R_m can be split to different contributions assigned to atoms, groups of atoms or even single bonds. Equation (4) describes how the refractive index n increases with R_m/V_m. So, the introduction of atoms or groups with high molar refraction would increase R_m/V_m, resulting in an increase of the refractive index n. According to the Ref. [14], R_m(C=C) = 1.733 cm^3/mol and R_m (Br) = 8.865 cm^3/mol were determined. Therefore, the Br-modification of v-SiO_2 connected with the reaction $-CH{=}CH_2 + Br_2 \rightarrow -CHBr{-}CH_2Br$ will very effectively increase the refractive index, leading to the observed red-shift of the Bragg peak.

As mentioned in the introduction, it is important to obtain volume-encapsulated Au-NPs which are stable at higher temperatures. Here we aimed to obtain Au-NPs in the SiO_2 shells using the strong interaction between Au and thiol group. An aqueous $HAuCl_4$ solution was added to the PS@mp-SiO_2 particles at 80 °C. We observed a slightly pink milky suspension with a layer of solid particles on the bottom of the reaction vessel. We ascribe this layer to particles with a large amount of gold on the outer surface (see Fig. S3). They likely became too heavy and precipitated to the bottom. The majority of the particles, however, remained in the suspension.

In the next step, 0@Au-NP:SiO_2 shells were obtained by calcination of the Au-impregnated PS@mp-SiO_2 core–shell particles at 550 °C for 6 h. In this process, the PS core and organic part in the shells were removed. Therefore, we name the core part in 0@ … with the sign zero. The samples were characterized by scanning transmission electron microscopy using the normal secondary electron mode (SE) but also dark field transmission mode (DF) and transmission bright field mode (BF).

We assign the Au-NPs to volume-incorporated and surface-adsorbed ones. This interpretation can be visualized in an EM composite image (Fig. 5). The image shows the two different Au-NPs in two colors: green – the incorporated Au, and yellow – the Au at the outer surface. The individual shell particle in Fig. 5 (also see Fig. S4) was chosen by demonstration reasons to show both

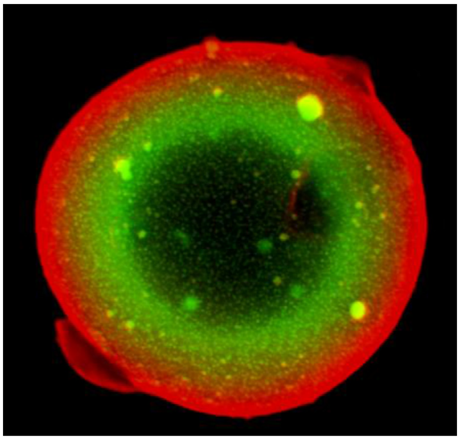

Fig. 5. Electron microscopic composite image of a selected 0@Au-NP:SiO_2 shell. The red component was generated by the DF signal and the green one by the SE signal simultaneously recorded. The logic operation applied to the two original component RGB-pictures was ADD. Therefore, the color change green-yellow-orange-red indicates the relative magnitude of the two components. The color of the small particles turns from green to yellowish-green if the particles are more near to the surface. Particles on the outer surface show a pale yellow color since they generate both signals with comparable magnitude. A red rim region is also visible which is nearly free of the color green, i.e. free of Au-NPs. (For interpretation of the references to color in this figure legend, the reader is referred to the web version of this article.)

types of Au-NPs. Most of the 0@Au-NP:SiO_2 shells do not show any Au-NP at the outer surface. Therefore, most of the Au formed in this synthesis is encapsulated which should be useful for many functions and surface decoration remains an exception only.

To get more quantitative information on the distribution of the Au-NPs in the SiO_2 shell, sections of the sample were made with an ultra-microtome. The samples were studied electron-microscopically (Fig. 6, S6, and S7). As visible in Fig. 6a, the Au-NPs are indeed well distributed inside the SiO_2 shell, seemingly with a slight gradient. EDX mapping of the O, Si, and Au are shown in Fig. 6b and confirm this impression. The plot in Fig. 6a shows the distribution of O, Si, and Au inside the shell with a maximum of Au near the outer surface and a clear penetration into the shell interior. The EDX analysis showed an average loading of 20.8 wt% Au-NPs in the SiO_2 shells (Fig. S5), which has potential application in the high-temperature catalytic reactions. More images of 0@Au-NP:SiO_2 shells are given in the Supporting Information. The Au-NP size distribution in the SiO_2 shell was measured as shown in Fig. S8 delivering a size range from 1 nm to 5 nm with an average of (2.2 ± 0.5) nm.

According to the above results, we propose the following formation mechanism for the gold in 0@Au-NP:SiO_2: (1) Au^{3+} ions are soaked-in into the mp-SiO_2 shell together with the solvent; (2) Some of the Au^{3+} ions are converted to Au^0 and formed small Au-NPs (<1 nm); (3) the rest of the Au^{3+} is decomposed to Au^0 (normally at 300 °C) [18,35] migrating at this temperature and leading to further growth of the small Au-NPs up to 1–5 nm. The occasional big Au-NPs on the outer surface of some particles, we ascribe to the nucleation (reduction of Au ions) and growth on the outer surface.

In this mechanism, the originally synthesized functionalized shells fulfill several functions. They allow the transport of the Au ions, reduce a part of the Au precursor, and act as a support confining the growth of the Au-NPs throughout the whole high temperature treatment. This combination of functions allows the high-percentage encapsulation of Au-NPs inside the SiO_2 shells during a high temperature treatment, which is essential for the stability of the system. Mesoporous SiO_2 has already been discussed as a promising support for Au-NPs, but the Au-NPs can break the silica pore walls and overgrow the pore size at temperatures of about 200 °C [18,22]. It was suggested [18] that the thickness of the walls in mesoporous SiO_2 is too thin to prevent the migration of Au particles. The SiO_2 matrix obtained by calcination of mp-SiO_2, however, turned out to be stable and dense enough to restrict the migration of Au-NPs. To use the particles for catalytic applications, further measurements such as pore size distribution and pore volume will be carried out. This could be a separate work which is still in progress.

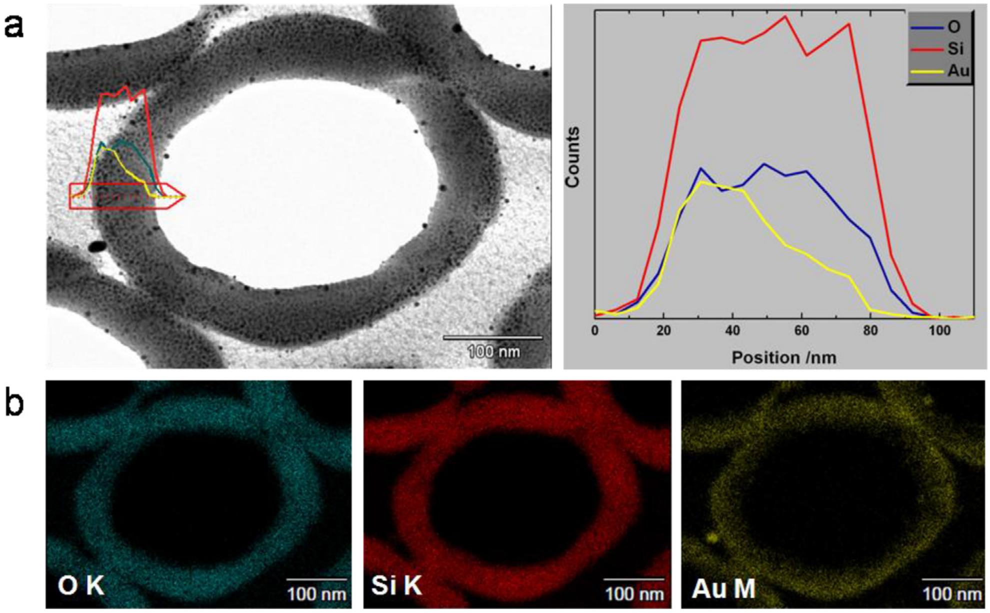

Fig. 6. (a) Electron microscopic BF image of a 0@Au-NP:SiO_2 shell. The microtome section has a thickness of about 28 nm. The plot shows the distribution of each element (O, Si, and Au) through the arrow direction (from outer surface to inner surface). (b) EDX mapping of the element distribution of O (left), Si (middle), and Au (right) on this section. Studies on other particles and other positions are shown in the Supporting Information.

4. Conclusions

In summary, we have developed a method of one-step organosilica coating on PS particles, and their application as tunable photonic band gap materials and support for Au nanoparticles. The organic functional groups have been varied among methyl, propyl, vinly, and mercaptopropyl. The PS@v-SiO_2 colloidal crystals were modified with bromine, resulting in tunable stop band. The increase of the refractive index of the shell is large ($\Delta n_{sh} = 0.17$) and leads to a significant shift of the Bragg peak. This big change of n_{sh} offers usable tuning possibilities for colloidal crystals. The whole crystal could be changed or also localized regions needed in designing hetero-structures for photonics. The modification of functionalized PS@organo-SiO_2 particles might be extended to treatments with hydroboron. The second modification has led to Au-NPs encapsulated inside the SiO_2 shell with a loading ratio of about 20 wt%. The Au-NPs occur in the whole SiO_2 shell and they are stable at 550 °C.

The direct organo-silica coating has the general advantage of an inherently homogeneous distribution of the functional groups, in comparison with post-synthesis grafting. Therefore, it could be a key method for the construction of complex functional nanostructures.

Acknowledgment

The authors thank Bernd Spliethoff for his extensive electron microscopy work and useful discussions.

Appendix A. Supplementary data

Supplementary data related to this article can be found at http://dx.doi.org/10.1016/j.matchemphys.2015.06.027.

References

[1] F. Hoffmann, M. Cornelius, J. Morell, M. Fröba, Silica-based mesoporous organic–inorganic hybrid materials, Angew. Chem. Int. Ed. 45 (2006) 3216–3251.
[2] H. Zou, S. Wu, J. Shen, Polymer/silica nanocomposites: preparation, characterization, properties, and applications, Chem. Rev. 108 (2008) 3893–3957.
[3] A. Guerrero-Martínez, J. Pérez-Juste, L.M. Liz-Marzán, Recent progress on silica coating of nanoparticles and related nanomaterials, Adv. Mater. 22 (2010) 1182–1195.
[4] R.G. Chaudhuri, S. Paria, Core/shell nanoparticles: classes, properties, synthesis mechanisms, characterization, and applications, Chem. Rev. 112 (2012) 2373–2433.
[5] J.L. Vivero-Escoto, R.C. Huxford-Phillips, W. Lin, Silica-based nanoprobes for biomedical imaging and theranostic applications, Chem. Soc. Rev. 41 (2012) 2673–2685.
[6] F. Marlow, Muldarisnur, P. Sharifi, R. Brinkmann, C. Mendive, Opals: status and prospects, Angew. Chem. Int. Ed. 48 (2009) 6212–6233.
[7] F. Caruso, R.A. Caruso, H. Möhwald, Nanoengineering of inorganic and hybrid hollow spheres by colloidal templating, Science 282 (1998) 1111–1114.
[8] I. Tissot, J.P. Reymond, F. Lefebvre, E. Bourgeat-Lami, SiOH-functionalized polystyrene latexes. A step toward the synthesis of hollow silica nanoparticles, Chem. Mater. 14 (2002) 1325–1331.
[9] C. Graf, D.L.J. Vossen, A. Imhof, A.v Blaaderen, A general method to coat colloidal particles with silica, Langmuir 19 (2003) 6693–6700.
[10] Y. Lu, J. McLellan, Y. Xia, Synthesis and crystallization of hybrid spherical colloids composed of polystyrene cores and silica shells, Langmuir 20 (2004) 3464–3470.
[11] G. Qi, Y. Wang, L. Estevez, A.K. Switzer, X. Duan, X. Yang, E.P. Giannelis, Facile and scalable synthesis of monodispersed spherical capsules with a mesoporous shell, Chem. Mater. 22 (2010) 2693–2695.
[12] W. Stöber, A. Fink, E. Bohn, Controlled growth of monodisperse silica spheres in micron size range, J. Colloid Interface Sci. 26 (1968) 62–69.
[13] B. Sun, S.A. Mutch, R.M. Lorenz, D.T. Chiu, Layered polyelectrolyte–silica coating for nanocapsules, Langmuir 21 (2005) 10763–10769.
[14] D. Gan, L.A. Lyon, Tunable swelling kinetics in core-shell hydrogel nanoparticles, J. Am. Chem. Soc. 123 (2001) 7511–7517.
[15] L. Wang, S.A. Asher, Fabrication of silica shell photonic crystals through flexible core templates, Chem. Mater. 21 (2009) 4608–4613.
[16] C.-m Yang, M. Kalwei, F. Schüth, K.-j Chao, Gold nanoparticles in SBA-15 showing catalytic activity in CO oxidation, Appl. Catal. A Gen 254 (2003) 289–296.
[17] M. Bandyopadhyay, O. Korsak, M.W.E.v.d Berg, W. Grünert, A. Birkner, W. Li, F. Schüth, H. Gies, Gold nano-particles stabilized in mesoporous MCM-48 as active CO-oxidation catalyst, Microporous Mesoporous Mater. 89 (2006) 158–163.
[18] C.-K. Tsung, W. Hong, Q. Shi, X. Kou, M.H. Yeung, J. Wang, G.D. Stucky, Shape- and orientation-controlled gold nanoparticles formed within mesoporous silica nanofibers, Adv. Funct. Mater. 16 (2006) 2225–2230.
[19] Y. Piao, A. Burns, J. Kim, U. Wiesner, T. Hyeon, Designed fabrication of silica-based nanostructured particle systems for nanomedicine applications, Adv. Funct. Mater. 18 (2008) 3745–3758.
[20] Z. Lu, J. Goebl, J. Ge, Y. Yin, Self-assembly and tunable plasmonic property of gold nanoparticles on mercapto-silica microspheres, J. Mater. Chem. 19 (2009) 4597–4602.
[21] M. Sanles-Sobrido, W. Exner, L. Rodríguez-Lorenzo, B. Rodríguez-González, M.A. Correa-Duarte, R.A. Álvarez-Puebla, L.M. Liz-Marzán, Design of SERS-encoded, submicron, hollow particles through confined growth of encapsulated metal nanoparticles, J. Am. Chem. Soc. 131 (2009) 2699–2705.
[22] H. Kumagi, K. Yano, Synthesis and characterization of Au-loaded core/shell mesoporous silica spheres containing propyl group in the shell, Chem. Mater. 22 (2010) 5112–5118.
[23] L. Tan, D. Chen, H. Liu, F. Tang, A silica nanorattle with a mesoporous shell: an ideal nanoreactor for the preparation of tunable gold cores, Adv. Mater. 22 (2010) 4885–4889.
[24] Z. Lu, C. Gao, Q. Zhang, M. Chi, J.Y. Howe, Y. Yin, Direct assembly of hydrophobic nanoparticles to multifunctional structures, Nano Lett. 11 (2011) 3404–3412.
[25] T.S. Deng, F. Marlow, Synthesis of monodisperse polystyrene@vinyl-SiO_2 core–shell particles and hollow SiO_2 spheres, Chem. Mater. 24 (2012) 536–542.
[26] T.S. Deng, Q.F. Zhang, J.Y. Zhang, X. Shen, K.T. Zhu, J.L. Wu, One-step synthesis of highly monodisperse hybrid silica spheres in aqueous solution, J. Colloid Interface Sci. 329 (2009) 292–299.
[27] T.S. Deng, P. Sharifi, F. Marlow, Opal shell structures: direct assembly versus inversion approach, ChemPhysChem 14 (2013) 2893–2896.
[28] S. Dash, S. Mishra, S. Patel, B.K. Mishra, Organically modified silica: synthesis and applications due to its surface interaction with organic molecules, Adv. Colloid Interface Sci. 140 (2008) 77–94.
[29] Y.B. Kim, Y.-A. Kim, K.-S. Yoon, Preparation of functionalized polysilsesquioxane and polysilsesquioxane-metal nanoparticle composite spheres, Macromol. Rapid Commun. 27 (2006) 1247–1253.
[30] S.S.M. Lee, J.H.K.W. Choi, Preparation and characterization of surface-functionalized polysilsesquioxane hard spheres in aqueous medium, Macromolecules 41 (2008) 6195–6204.
[31] E.M. Brozek, I. Zharov, Internal functionalization and surface modification of vinylsilsesquioxane nanoparticles, Chem. Mater. 21 (2009) 1451–1456.
[32] T.S. Deng, J.Y. Zhang, K.T. Zhu, Q.F. Zhang, J.L. Wu, Temperature-modified photonic bandgap in colloidal photonic crystals fabricated by vinyl functionalized silica spheres, Mater. Chem. Phys. 129 (2011) 540–546.
[33] P. Brocos, Á. Piñeiro, R. Bravo, A. Amigo, Refractive indices, molar volumes and molar refractions of binary liquid mixtures: concepts and correlations, Phys. Chem. Chem. Phys. 5 (2003) 550–557.
[34] M.F. Roll, P. Mathur, K. Takahashi, J.W. Kampf, R.M. Laine, [PhSiO1.5]8 promotes self-bromination to produce [o-BrPhSiO1.5]8, J. Mater. Chem. 21 (2011) 11167–11176.
[35] K. Kuge, G. Calzaferri, Gold-loaded zeolite A, Microporous Mesoporous Mater. 66 (2003) 15–20.